Geochemistry Geophysics Geosystems G3
AN ELECTRONIC JOURNAL OF THE EARTH SCIENCES
Published by AGU and the Geochemical Society

Article
Volume 10, Number 1
31 January 2009
Q01010, doi:10.1029/2008GC002121
ISSN: 1525-2027

Seismic and drilling constraints on velocity structure and reflectivity near IODP Hole U1309D on the central dome of Atlantis Massif, Mid-Atlantic Ridge 30°N

John A. Collins
Department of Geology and Geophysics, Woods Hole Oceanographic Institution, Woods Hole, Massachusetts 02543, USA

Donna K. Blackman
Scripps Institution of Oceanography, University of California, San Diego, La Jolla, California 92093, USA (dblackman@ucsd.edu)

Amber Harris
Graduate School of Oceanography, University of Rhode Island, Narragansett, Rhode Island 02882, USA

Richard L. Carlson
Department of Geology and Geophysics, Texas A&M University, College Station, Texas 77843, USA

[1] The seismic structure of the upper ~1 km of the central dome of Atlantis Massif is investigated in the context of lithologies known from seafloor drilling and physical property measurements obtained within the borehole and on core samples. A new analysis of seafloor refraction data and multichannel reflection data acquired in the immediate vicinity of Integrated Ocean Drilling Program (IODP) Site U1309 was motivated by a discrepancy between initial seismic interpretations, which indicated mantle velocities at shallow depth, and the gabbroic sequence recovered by drilling. A new seismic velocity model is derived that is consistent with the full suite of geological and geophysical data in the central dome area; all of these data show that mafic intrusive rocks dominate the upper portion of the footwall of this oceanic core complex and that laterally extensive zones of ultramafic rocks are not required by the data. The origin of subseafloor reflectivity beneath the central dome was also considered. We find that seafloor scattering complicates the interpretation of multichannel seismic data acquired near Site U1309 but that detectable subsurface impedance contrasts do occur. Downhole variations in alteration may generate reflections observed from the upper kilometer of the central dome.

Components: 6713 words, 8 figures, 1 table.

Keywords: Atlantis Massif; IODP; oceanic core complex; marine seismics.

Index Terms: 7245 Seismology: Mid-ocean ridges; 7220 Seismology: Oceanic crust; 3036 Marine Geology and Geophysics: Ocean drilling.

Received 10 June 2008; **Revised** 26 November 2008; **Accepted** 26 December 2008; **Published** 31 January 2009.

Collins, J. A., D. K. Blackman, A. Harris, and R. L. Carlson (2009), Seismic and drilling constraints on velocity structure and reflectivity near IODP Hole U1309D on the central dome of Atlantis Massif, Mid-Atlantic Ridge 30°N, *Geochem. Geophys. Geosyst.*, *10*, Q01010, doi:10.1029/2008GC002121.

1. Introduction

[2] Knowledge of the distribution of rock type and alteration within the domal core of Atlantis Massif constrains models of the development of oceanic core complexes (OCC), specifically the interplay between detachment faulting and magmatism associated with their formation. OCC are hypothesized to reflect a mode of lithospheric construction that is at least episodic [*Tucholke and Lin*, 1994; *Cann et al.*, 1997; *Tucholke et al.*, 1998; *Escartín et al.*, 2003] and in some areas may even be common [*Okino et al.*, 2004; *Smith et al.*, 2006], particularly at slow spreading centers, where magma supply is inferred to vary significantly in both space and time. Prior to drilling, seafloor geology and initial geophysical analyses suggested that the domal core unroofed by a detachment fault at Atlantis Massif was dominated by ultramafic rock. However, the recovery of a gabbroic sequence from Integrated Ocean Drilling Program (IODP) Hole U1309D suggests that this OCC is similar to other oceanic detachment systems where the footwall has been drilled such as the Atlantis Bank [*Dick et al.*, 2000] and 15°45′N Mid-Atlantic Ridge [*Kelemen et al.*, 2004; *MacLeod et al.*, 2002]. The ground truth provided by deep drilling at Atlantis Massif motivated a reappraisal of seismic data acquired in the vicinity of IODP Site 1309.

2. Seismic Data in the Vicinity of IODP Site 1309

2.1. Seismic Refraction

[3] In 1997, a series of on-bottom (near-seafloor source and seafloor receiver) and conventional (sea surface source, seafloor receiver) refraction profiles were shot on the Atlantis Massif (Figure 1). For the former, the NOBEL near-bottom explosive source [e.g., *Christeson et al.*, 1994] was used to fire 10 lb charges immediately above the seafloor with a shot spacing of ~40 m over a profile length of ~2 km. Shot spacing for the air gun profiles was ~250 m. Here we present analyses of two on-bottom profiles, NOBEL9 and NOBEL10, that extend ~2 km across the top of the central dome of the massif. The NOBEL shots were recorded by receivers located at both ends of the profile, thus producing reversed refraction profiles. Plotted using a reduction velocity of 7.5 km/s (Figure 2), each record section shows at least a short interval where first arrivals have a flat slope, which in a horizontally stratified earth would imply a layer velocity of 7.5 km/s.

2.2. Seismic Reflection

[4] Five multichannel seismic (MCS) reflection profiles were obtained in 2001 by the R/V *Ewing* (cruise EW0102) using a 6-km streamer and an air gun shot spacing of 37.5 m (Figure 1). Initial processing by *Canales et al.* [2004] included predictive deconvolution, dip moveout-based suppression of scattering, stacking, finite difference time migration, bandpass filtering, and muting below the water multiple. The resulting sections show a prominent seismic event, designated the "D" reflector (Figure 3), which was interpreted as a reflection from either an alteration front or a subsurface detachment zone. Here, we analyze common midpoint (CMP) gathers and a portion of CMP stacked data from line Meg4 where it is closest (~400 m) to Hole U1309D and compare these data with predictions from synthetic reflectivity modeling based on measurements made in the hole.

2.3. Integrated Ocean Drilling Program Hole U1309D

[5] Integrated Ocean Drilling Program Hole U1309D penetrated 1415 m into the central dome (Figure 1) and recovered a dominantly gabbroic sequence (Figure 4a) [*Blackman et al.*, 2006]. Alteration, via reaction with seawater, is pervasive in the upper few hundred meters of the core, but the lower part of the section, particularly at depths greater than 800 m below seafloor (mbsf), has several intervals with very little alteration (Figure 4b). Instances of alteration of the recovered core being 50% or greater are very rare below 750 mbsf (except in the 1080–1200 mbsf interval) but are common at shallower depths. By depths of 800 mbsf, instances of 40% or higher overall alteration are uncommon. By 850 mbsf, many instances of <10% alteration are reported (although less common in the 1080–1200 mbsf interval). Throughout, intervals with higher olivine content (e.g., olivine-rich troctolites) show greater overall alteration than surrounding lithologies (gabbro and less common diabase). Seismic data (check shot and wall rock logging) were obtained in the upper 800 m of the borehole (Figures 4e and 4g); poor weather precluded the final seismic logging runs that would have covered the 800–1400 m subseafloor interval.

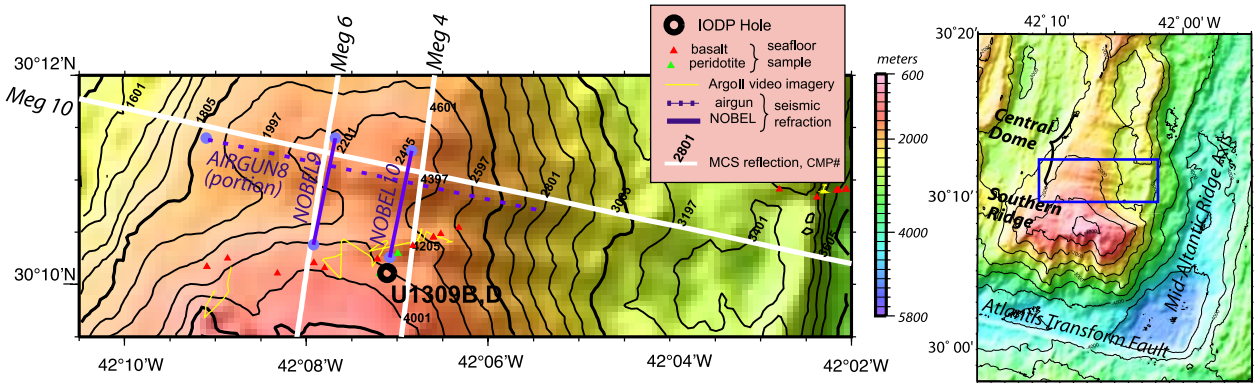

Figure 1. Locations of the IODP Site 1309 deep drill holes (B and D are 20 m apart, 101 m and 1415 m penetrations, respectively) on the Atlantis Massif and the seismic profiles discussed here. The "NOBEL9" and "NOBEL10" profiles are refraction profiles acquired with ocean-bottom hydrophones (OBH) and seafloor explosive shots. The refraction profile labeled "AIRGUN8" was acquired with air gun shots and a mix of ocean-bottom seismographs (OBS) and OBH. Blue dots show OBS/H locations. Lines "Meg10" and "Meg4" are two common-midpoint-point reflection profiles. The tectonic setting of the drill hole and seismic profiles is shown on the index map at right, where the blue box shows the location of the drill site map.

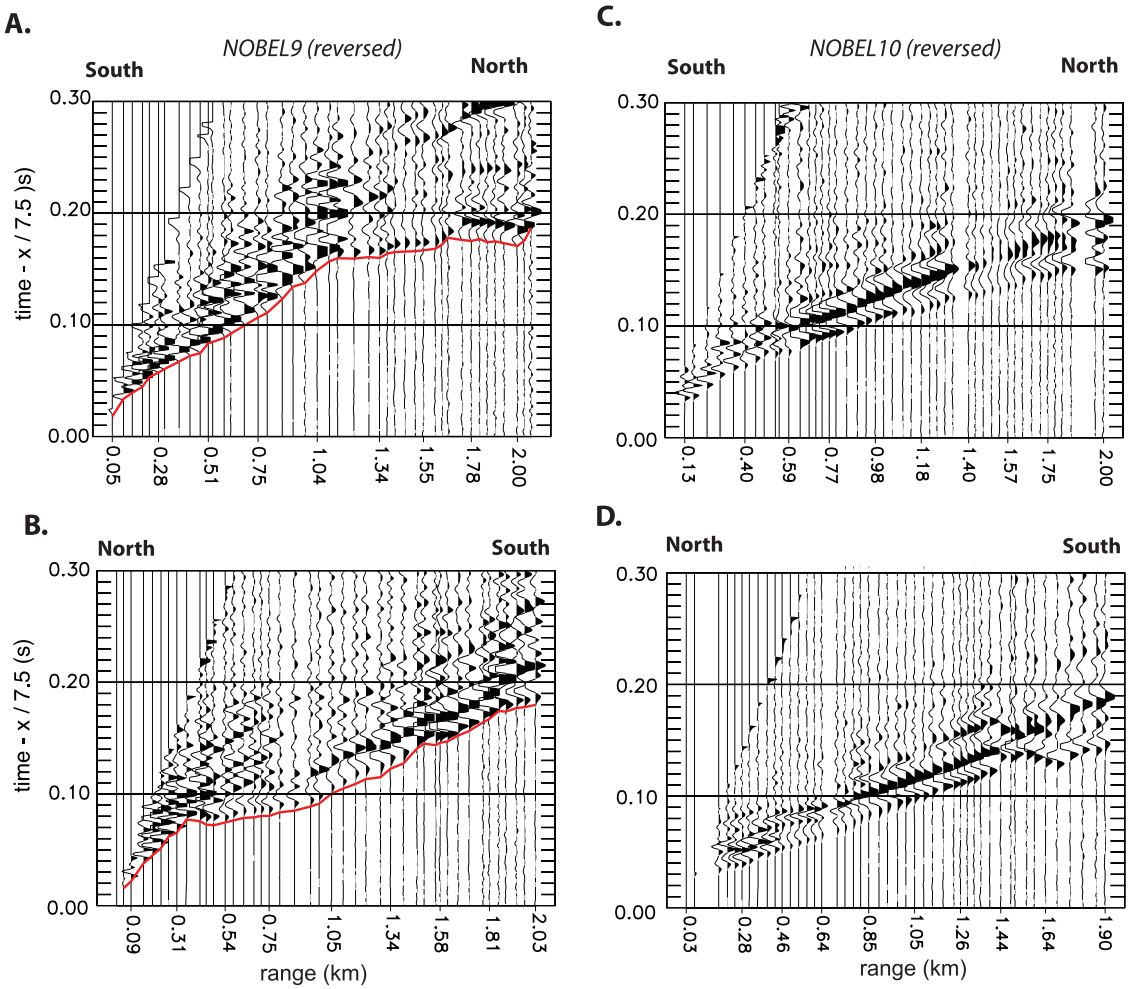

Figure 2. Seismic record sections for the (a and b) NOBEL9 and (c and d) NOBEL10 on-bottom refraction profiles shot on the massif. The red lines in Figures 2a and 2b show the traveltime picks used to derive one of two velocity models for NOBEL9.

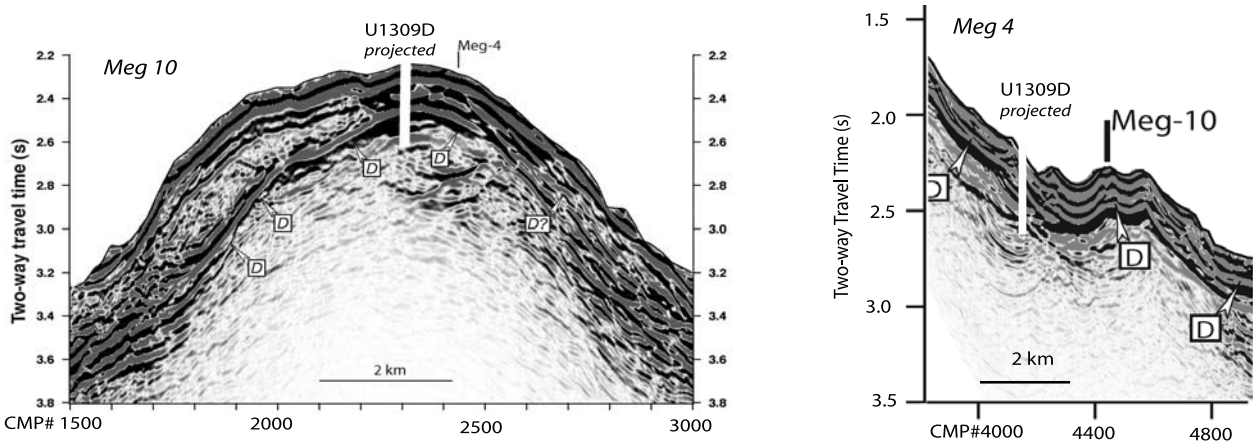

Figure 3. Multichannel seismic (MCS) reflection profiles from the central dome of the Atlantis Massif [from *Canales et al.*, 2004]. Note the location of the projection of IODP Hole U1309D onto these lines.

2.4. Check Shot Seismics

[6] The drill ship deployed a three-component wireline seismometer in Hole U1309D, clamping the instrument in place for 1 kHz recording at ~50 m intervals from 250 to 800 mbsf [*Blackman et al.*, 2006]. A 150 cubic inch GI gun was deployed from the ship, at depths varying from 0 to 2 m below sea surface because of heave in moderate seas. Ten to twenty shots were fired to each borehole station. A number of noisy traces (due to drill pipe hitting against the side of the upper part of the hole) were

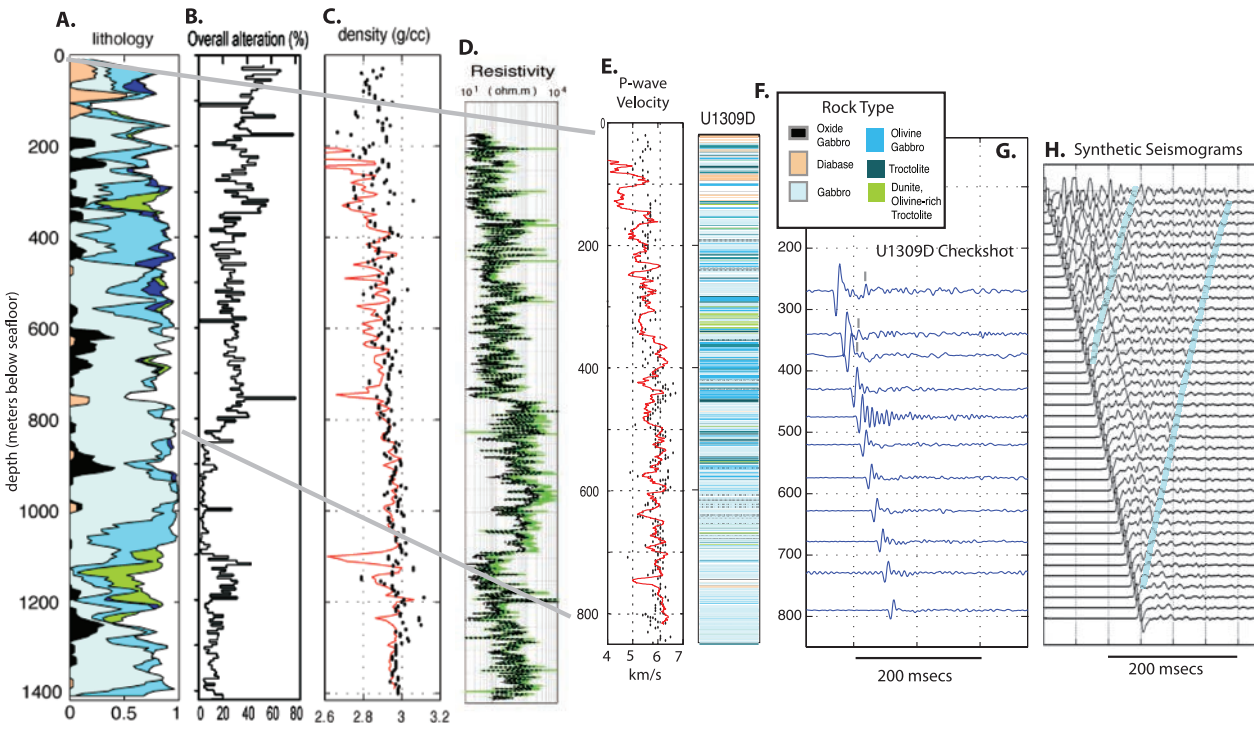

Figure 4. Downhole data at IODP Hole U1309D. (a) Lithology column shows dominantly gabbroic section and intervals with greater olivine content. (b) Alteration was estimated during shipboard visual core description. (c) Red curves show logged density; black dots are shipboard core sample measurements. (d) Wall rock resistivity measured by borehole logging. (e) Downhole velocity logged in wall rock (red) and core sample measurements at room pressure (black dots). (f) Expanded view of lithology in upper 800 m of section. (g) Check shot seismograms show strong first arrival but later arrivals are only visible in the subsequent ~75 ms in the upper four to five traces. (h) Synthetic VSP seismograms calculated using borehole values of velocity and density show low-amplitude reflection events highlighted by the light blue curve. Other events are also visible.

Table 1. Check Shot Cross-Correlation Summary

Station	Depth (mbsf)	Lag (s)	Error (s)
1	272	−0.04253	0.000022
2	342	−0.03048	0.000021
3	377	−0.02429	0.000032
4	432	−0.01449	0.000026
5	477	−0.00600	0.000031
6	522	0.00000	0.000008
7	576	0.00863	0.000034
8	630	0.01738	0.000019
9	680	0.02653	0.000028
10	731	0.03465	0.000025
11	792	0.04366	0.000033

eliminated. Small (<4 ms) shifts due to the slightly variable source-receiver spacing were determined by cross-correlation of the first arrival pulses and corrections were applied prior to stacking of the remaining traces. The seismograms were filtered with a 5–120 Hz bandpass filter (Figure 4g).

[7] A cross-correlation method was used to measure relative arrival times between borehole stations with a precision of 0.02–0.03 ms. The lags relative to a reference trace (recorded at the station 522 mbsf where the arrival has a particularly 'clean' first pulse) were determined following the method described by *Carlson* [2004]. A nine-point correlation of each record was computed with the first half cycle of the first arrival of the reference trace. A quadratic function was fit to the five points bracketing the maximum correlation value and then the best-fit lag (Table 1) was determined from the derivative of that quadratic function for each station. The best-fit single line through the data has slope corresponding to an average velocity of 6.03 ± 0.05 km/s. However, fitting separate curves through the upper and lower intervals improves the fit to the values shallower than 500 mbsf (Figure 5) and indicates velocity averages 5.62 ± 0.03 km/s in the 272–477 mbsf interval and 6.01 km/s in the 522–792 mbsf interval. This division into upper and lower intervals produces check shot velocities that are similar to the logged wall rock velocities, as discussed in section 2.5.

2.5. Borehole Logs

[8] A Schlumberger sonic logging tool was used to measure compressional and shear wave velocity of the wall rock. Formation density was obtained using a litho-density tool (see Methods section in the work of *Blackman et al.* [2006]). The overall hole condition was good but a number of small intervals had caliper readings more than 3 inches beyond bore, where velocity measurements are probably unreliable. A 10-m running average was taken to reduce noise associated with such lower-quality measurements (Figures 4c and 4e). Wall rock velocity at the few-meter scale sensed by the logging tool averages 5.6 km/s in the upper ~500 m. This value is consistent with the fit to the check shot data from this interval. The average wall rock velocity in the 500–800 m interval is 6.0 km/s, slightly lower, but also in good statistical agreement with the average determined from the check shot survey. A more detailed analysis suggests that both the overall trend of the sonic log and the check shot traveltimes are consistent with compression of large-scale cracks in the gabbro under increasing overburden pressure [*Carlson et al.*, 2008].

2.6. Core Sample Velocity Measurements

[9] Samples measuring about 8 cm^3 were taken from unfractured sections of the recovered core, resaturated under vacuum in seawater for 24 h, and their velocity measured at room temperature and pressure [*Blackman et al.*, 2006] (Figure 4e, black dots). To determine the sample velocities under simulated in situ conditions, a second set of velocity measurements was made onshore at elevated

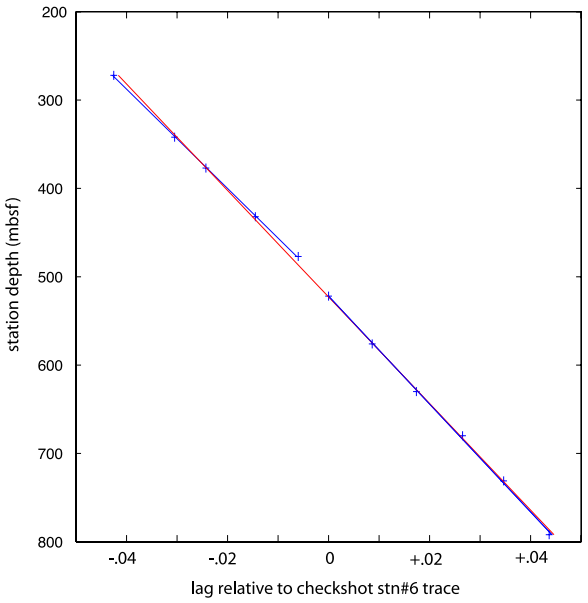

Figure 5. The vertically averaged seismic velocity at Hole U1309D is derived by a linear fit between traveltime lag and station depth. The single curve corresponds to Vp of 6.03 ± 0.05 km/s. The two-line fit gives velocities of 5.62 km/s and 6.01 km/s in the upper and lower sections of the borehole, respectively.

hydrostatic pressures to 200 MPa. For these measurements, core samples were selected from 250 to 400 mbsf and 700–900 mbsf based on core descriptions (alteration changes) and log data (Vp and resistivity changes, Figures 4d–4e). We focused on these intervals because they potentially correlated with the traveltimes of reflection events observed in the MCS data.

[10] Velocity measurements at in situ pressure were obtained in the lab at Texas A&M University [*Willson et al.*, 2007]. Minicores and cubes were subsampled to produce smaller minicores (18.275 mm diameter) to match the size of instrument electrodes. The ends of the new minicores were polished to create a better contact surface. Samples were saturated in a standard seawater solution then wrapped in a copper mesh, followed by a copper sheath, both affixed with copper tape, and the sample was placed within a rubber tube. Standard seawater was swabbed onto the end surfaces for better contact with the electrodes, which were placed into the rubber tube. The sample was sealed by copper wire twisted around the outside of the rubber tube at the electrode ends of the tube in order to prevent the pressure vessel fluid from entering the sample. The pressure within the vessel was controlled by the amount of silicon oil pumped into or released from the chamber. Silicon oil was chosen because its low viscosity helped shorten equilibration time, but this also makes keeping the oil from the sample more difficult. A signal was transmitted to one electrode, through the sample to the other electrode, and back to an oscilloscope. Using standards, a time delay for the system was calculated and measurements were adjusted to compensate for the circuit time loss. The received waveform was recorded and a first break time arrival was hand picked. Velocity was calculated for a set of pressure conditions (0, 0.5, 2, 5, 10, 20, 40, 60, 80, 100, 140, 180, 200 MPa), both while pressure was increasing and decreasing. For the data reported here, velocity was determined for increasing pressure, presumed most accurate due to the difficulty of fluids moving back into sample pore space once pressed out. We iteratively fit a curve to the data following the "bed of nails" model reported by *Carlson and Gangi* [1985]. The curve fitting helps to predict a more accurate value for the velocity at atmospheric pressure. The model curve is then used to determine in situ velocity at the pressure appropriate for the depth of each sample (blue squares, Figure 6). A hydrostatic pressure increase with depth (20 MPa/km) was assumed appropriate on the basis of evidence of faulting and hydrothermal alteration in the recovered section.

[11] The velocities measured at in situ pressure are consistently higher than all other measures of seismic velocity in the vicinity of Site U1309, indicating that unfractured and fairly fresh samples have velocities of ~7.0 km/s. *Carlson and Miller* [2004] report similar results for other cored mafic oceanic rocks. The few samples with lower velocity at in situ pressure (5.8–6.3 km/s) are generally from portions of the core that have higher olivine content, and correspondingly greater overall alteration (Figures 4b and 6), in particular in the 310–335 mbsf interval (note that an oxide gabbro sample from a unit interfingered within that interval has higher velocity). This difference was not apparent from the room pressure measurements. If the four (in situ) lower-velocity samples are representative of most of the interval where olivine-rich troctolites are common (~310–335 mbsf), its thickness is just great enough to have an impact on the impedance contrast sensed at seismic wavelengths.

[12] For the 700–900 mbsf interval, the relative downhole velocities at in situ pressure were similar to the shipboard (atmospheric pressure) measurements in that there is no clear indication of a velocity jump. Thus any seismic reflector in that depth range cannot be explained in terms of inherent velocities of the mineral assemblages recovered from those portions of Hole U1309D.

3. Seismic Modeling

3.1. Full-Waveform Synthetic Seismograms

[13] The downhole log velocity and density data were used to calculate "synthetic" vertical seismic profile (VSP) seismograms for several source-receiver ranges that bracket the experimental geometry. Average Vp, Vs, and density for 5-m bins from 150 to 800 mbsf comprised the input model. The full-waveform synthetic profiles (Figure 4h) were calculated using the reflection matrix method of *Kennett* [1983] and a source waveform generated from a library of source signatures and appropriate for the GI gun used to carry out the actual check shot experiment (J. Diebold, personal communication, 2006). Two modest reflectors are predicted to occur ~400 mbsf and ~750 mbsf and a smaller amplitude event is predicted to arise from near 640 mbsf. The check shot data appear to record the former (gray bar locates this on the upper three seismograms, Figure 4g) but there is no

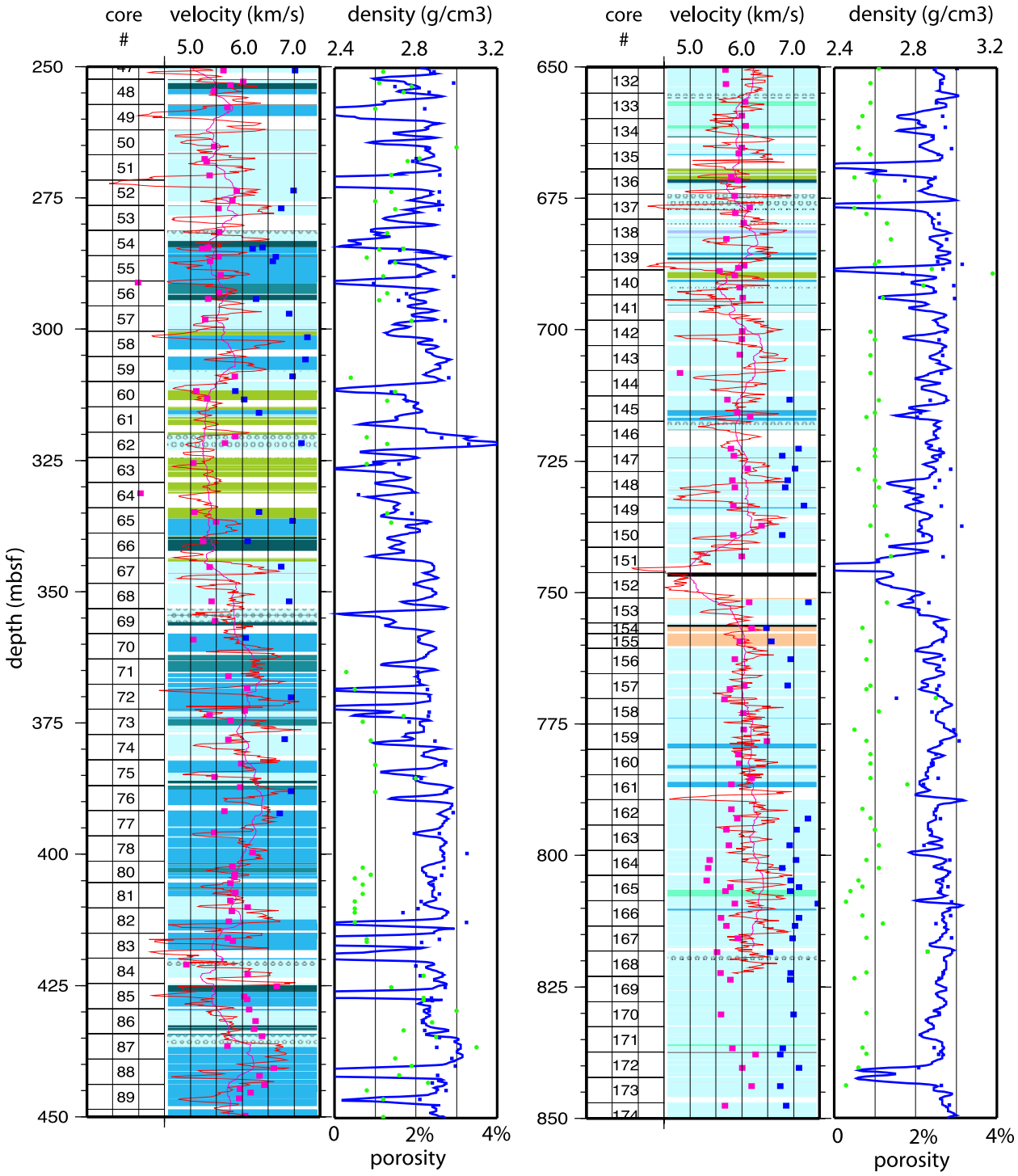

Figure 6. Lithology (color key as in Figure 4), borehole velocity (red line), core sample velocity (magenta dots: room T/P; blue dots: in situ P), borehole density (blue line), and core sample porosity (green dots), for two intervals in Hole U1309D where reflectivity modeling indicates impedance contrast.

evidence of anything similar to the latter two reflectors in the data. This could be due to low signal-to-noise ratio in that part of the seismogram. In addition, it is possible that the characterization of the 10–20 m interval centered on about 750 mbsf is misleading. *Michibayashi et al.* [2008] document evidence for faulting between 744 and 750 mbsf. An 80 cm length section of fault gouge was recovered in this interval, but the rest of the core barrel (4.2 m cored interval) was

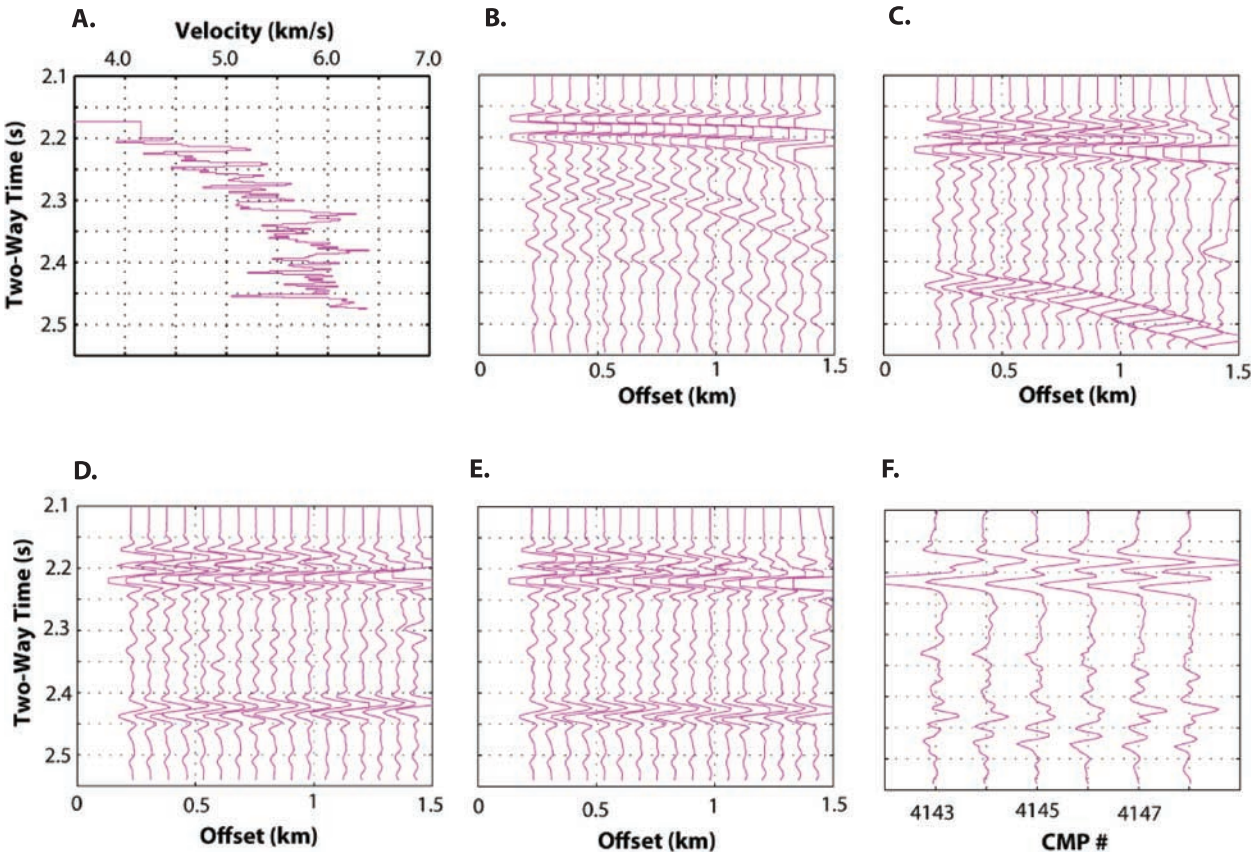

Figure 7. MCS modeling results and observed MCS data acquired near Hole U1309D. (a) The velocity model derived from the borehole logs. Here the model is shown as a function of two-way time in order to facilitate comparison between the model and the seismic data. (b) Synthetic normal-moveout (NMO) corrected CMP gather calculated for the earth model shown in Figure 7a. The NMO correction should result in true reflections having an approximately flat slope; the dipping arrivals are source bubble-pulse phases. (c) Observed CMP gather 4145 for MCS line Meg4. Filter (5–30 Hz) and NMO applied are the same as for synthetic in Figure 7b. Note the high-amplitude dipping phase with a near-vertical incidence arrival time of ~2.42 s. This strong event (relative to the seafloor reflection) is not predicted by the borehole logging data. (d) Observed CMP gather 4145 with NMO correction calculated for a constant stacking velocity of 1500 m/s. (e) Observed CMP gather 4145 with NMO correction calculated for a constant stacking velocity of 1560 m/s. (f) Stacked traces for several nearby CMP gathers from MCS line Meg4.

empty; that indicated a thin diabase unit. Calipers on one of the logging tools indicate that the borehole is several inches beyond bore in this interval so logged velocity and density measurements may be unreliable in this interval.

[14] The synthetic seismogram modeling does indicate that impedance contrasts observed in Hole U1309D would lead to internal reflectivity within the domal core. However, the amplitude predicted for the reflectors from the upper 800 mbsf is modest, in contrast to the prior depiction of a single, very strong D reflector occurring in that depth range [*Canales et al.*, 2004]. Further analysis of the MCS data in the vicinity of Site 1309 was conducted to determine what might contribute to this apparent discrepancy in the local region.

3.2. Slope Scatter Interference on MCS Near Hole U1309D

[15] Using the same earth model (Figure 7a) that we used for the VSP analysis, we calculated a synthetic CMP gather (Figure 7b) and compared it to the CMP gather from MCS line Meg4 closest to Hole U1309D (Figure 7c). The synthetic and observed gathers are plotted with a normal moveout (NMO) correction calculated for the velocity model shown in Figure 7a. The observed CMP gather (Figure 7c) shows a strong arrival at 2.42–2.55 s that is not predicted by the logging-derived earth model (Figure 7b). In order to assess the origin of the observed event, constant-velocity NMO-corrected gathers were plotted. Figures 7d and 7e show that the moveout of the event is "flat"

for a stacking velocity of 1560 m/s. This is only slightly above the speed of sound in water; thus we infer that this event is likely due to energy scattered off the slope where the southern ridge deepens toward the central dome near Site 1309. Stacked traces (Figure 7f) from several adjacent CMPs processed as in the work of *Canales et al.* [2004] indicate that this arrival is not attenuated by CMP stacking but appears as a single strong reflector at ~2.45 s on Meg4 where it is closest to Hole U1309D. Scattering from the slope ~800 m to the north of CDP 4145 could produce an event at the time observed in the stacked traces. The high impedance contrast at the seafloor where the scattering occurs could explain why this event has relatively high amplitude in the MCS data. It is much less reduced in amplitude relative to the actual seafloor reflector than are the reflectors predicted from the reflectivity modeling based on measured impedance contrasts in the borehole.

[16] It is possible that the low stacking velocity of the 2.45 s event is an effect due to a thin, low-velocity layer just below the seafloor. Refraction modeling (OBS, next section and MCS streamer analysis) [*Harding et al.*, 2007] indicates that a topmost layer with velocity 2.5–3 km/s occurs on at least parts of the massif dome. Reflections from the base of such a low-velocity layer would have modest stacking velocities. However, the ~100 m thickness determined for this layer in local areas to date is too small to explain an event with an ~0.25 s delay relative to the seafloor.

3.3. OBS Refraction

[17] The on-bottom refraction profiles (NOBEL9 and NOBEL10) were analyzed using both the 2-D traveltime tomographic technique of *Korenaga et al.* [2000] and the 2-D "layer-stripping" technique of *Zelt and Smith* [1992]. The data were recorded at a sample rate of 1000 Hz in order to adequately sample the high-frequency signals generated by the deep source, and first-arrival pick uncertainties are ±2 ms. Because the source shots were detonated just above, rather than on, the seafloor, the individually picked arrival times were first corrected for varying source height above the seafloor. The height of the source was derived using the height of NOBEL as measured by an altimeter and the known length of detonator cord between NOBEL and the explosive charge. The initial suite of refraction models tested (*Collins et al.* [2003] and presented herein) was guided by the documented predominance of serpentinized harzburgite, and lesser gabbro, on the southern wall of Atlantis Massif, in the kilometer immediately below the peak of Atlantis Massif [*Blackman et al.*, 2002]. The initial tomography-derived models for NOBEL9 and NOBEL10 are shown in Figures 8a and 8b. Both models show considerable lateral variations in velocity. The measured traveltimes for NOBEL9 are consistent with the presence of high-velocity rocks ($V_p \sim 7.5$ km/s) at subseafloor depths of about 600 m, comparable to the depth of reflector D in this area [*Canales et al.*, 2004]. NOBEL10, with model predictions also matching observed traveltimes to within pick uncertainty, do not require shallow high velocity. Both models require a thin (<100 m) uppermost layer with velocity ≤3 km/s to explain the near-offset arrivals. Note that the initial modeling for both of these NOBEL profiles assumed a flat seafloor.

[18] When almost no ultramafic rocks were recovered from Hole U1309D modeling efforts were renewed. Using the method of *Zelt and Smith* [1992], a series of forward ray tracing experiments was run to determine if NOBEL9 could be fit by a model including only velocities <6.5 km/s, as would be appropriate for mafic rocks. Indeed, including seafloor topography and somewhat greater variability in layer thickness along the line, a satisfactory fit to the data (RMS misfit 4 ms) is obtained (Figure 8c). The picks shown for NOBEL9 in Figure 2a are the ones used for the renewed modeling effort. Most of these picks are identical to those used in the initial modeling; however, in the 0.8–1.2 km portion of NOBEL9 arrivals that were associated with reflection off a floating horizon (assumed to correspond to a strong reflector D) are now associated with refracted arrivals. The smaller earlier arrivals (barely visible in Figure 2a with the plotting parameters employed) considered as signal in the earlier modeling are not included here; thus signal-to-noise ratio of considered picks is more consistent. The lack of a single, strong impedance contrast from in Hole U1309D suggests that while a reflector may occur in the 350–500 mbsf interval it probably is not as strong or isolated relative to others in the section as had been interpreted initially. This is why we focus on refracted arrivals in the new modeling of the NOBEL data.

[19] The shallow, low-velocity layer is somewhat greater in thickness for the alternate NOBEL9 model derived by the layer-stripping technique than in the earlier tomographic model. It is important to note that it is not merely the addition of

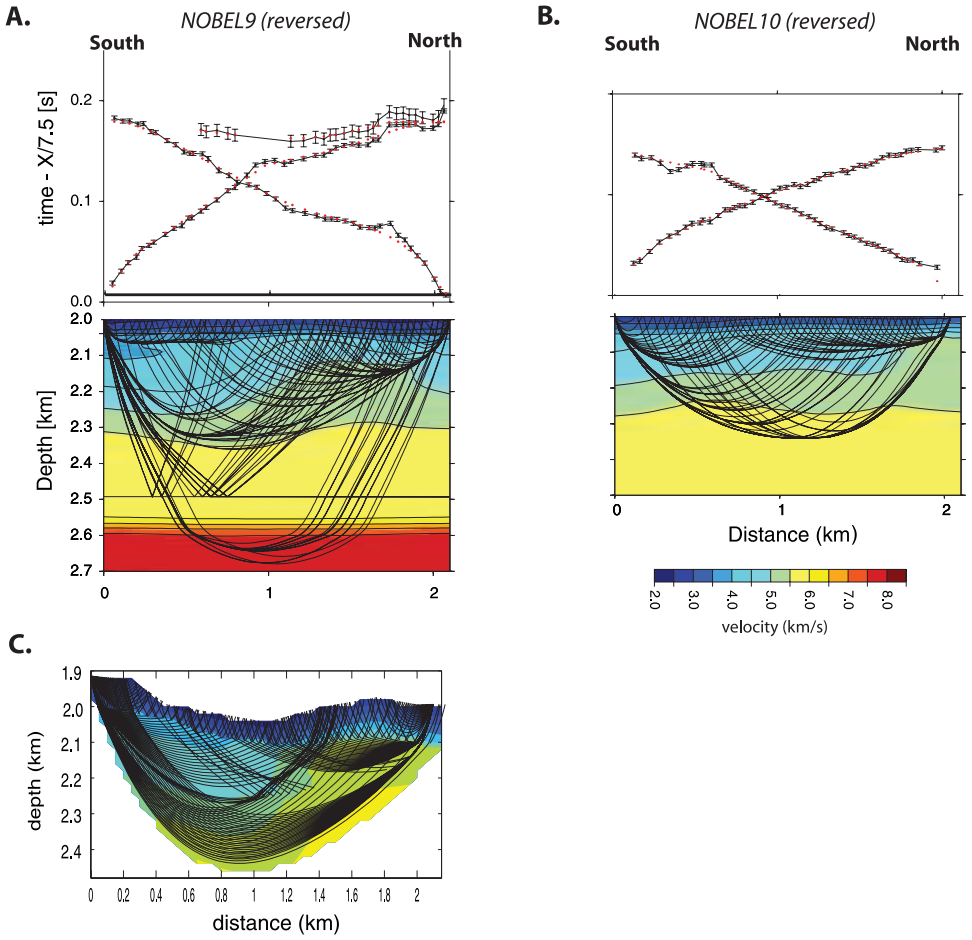

Figure 8. Refraction velocity models, observed (black circles with error bars) and predicted traveltimes (red circles) for on-bottom refraction profiles (a) NOBEL9 and (b) NOBEL10. The velocity models shown in Figures 8a and 8b were derived using the 2-D traveltime tomographic technique of *Korenaga et al.* [2000], and assumed a flat seafloor. (c) An alternative velocity model for NOBEL9 derived using the 2-D "layer-stripping" technique of *Zelt and Smith* [1992]. This alternative model incorporates the measured seafloor bathymetry and a moderately different set of traveltime picks than the model presented in Figure 8a. RMS misfit for the models in Figures 8a and 8c are comparable, namely, 3 ms and 4 ms, respectively.

seafloor topography that results in a model that matches the data well without a shallow mantle velocity layer. Models with the same seafloor topography as in Figure 8c have also been determined to fit the data when a shallow mantle (7.5 km/s) layer exists; for one case the average depth of such layer was 500 m. Thus, such a layer is allowed by the NOBEL9 data but it is not required. As is always the case, the seismic traveltimes do not provide a unique determination of the subsurface structure and these results underscore this basic geophysical tenet. However, the fact that the NOBEL lines are reversed does provide more robust indication of the nature of the lateral variability (note the similarity in along-line variation in Figures 8a and 8c). Comparison of NOBEL9 and NOBEL10 models (Figures 8a–8b) also suggest how structure may vary in the spreading-parallel direction, with the highest vertical velocity gradients occurring about half a kilometer further north in the eastern profile (NOBEL10) compared to where the highest gradients begin in the western profile (NOBEL9), which is about 1.5 km away.

[20] A velocity model along the lines of the alternate velocity model (Figure 8c), with no (unaltered) ultramafic velocities, also provides a reasonable traveltime fit to the air gun refraction profile that crosses the NOBEL profiles (AIR GUN8, Figure 1). The fact that both the alternate NOBEL9 model and the prior NOBEL10 model are consistent with drilling and logging results (and with much more detailed tomography based on MCS streamer refractions [*Canales et al.*, 2008;

Harding et al., 2007]) indicates that we have converged on a local model that satisfies all the available data.

4. Discussion

[21] Several types of data available at Atlantis Massif prior to drilling led to a preference for initial velocity models that included essentially unaltered mantle within the upper kilometer of the domal core: mantle harzburgites recovered by submersible from the upper southern wall of the massif (~5 km south of Hole U1309) [*Blackman et al.*, 2002]; a strong reflector which appeared quite continuous and distinct based on initial, standard MCS processing [*Canales et al.*, 2004]; sparse samples of serpentinized peridotite from the central dome [*Blackman et al.*, 2002]; a positive gravity anomaly associated with the core of the massif [*Blackman et al.*, 2002; *Nooner et al.*, 2003]. However, drilling clearly indicated that significant (kilometer-plus scale) bodies of gabbro are contained within the domal core, an observation similar to drilling results from other OCC [*Ildefonse et al.*, 2007]. The reanalysis of geophysical data that we present here indicates that an alternate interpretation that does not include the presence of ultramafic rocks can explain the gravity [*Blackman et al.*, 2008], and NOBEL and local air gun refraction data. The revised local seismic model is consistent between both NOBEL lines, with MCS tomography [*Canales et al.*, 2008; *Harding et al.*, 2007], and with constraints obtained by drilling/logging.

[22] Velocity variations of as much as 1 km/s are determined to occur over lateral distances of several hundred meters at depths of 100–400 mbsf (Figure 8). This lateral scale is of the same order as the scale of downhole variability in average geophysical signatures determined at IODP Hole U1309D (e.g., resistivity and velocity, Figures 4d, 4e, and 5). Our analysis suggests that the style or degree of alteration may be an important factor in controlling the shallow (<1 km) velocity structure since primary rock type does not correlate with measured velocity in the drilled section/formation. However, details of petrology/geochemistry of individual magmatic units could also play a role in the observed lateral velocity gradients. Both deep gabbroic sections drilled in the oceans (Hole U1309D and Hole 735B in a core complex in the Indian Ocean [*Dick et al.*, 2000]) have been interpreted as consisting of a small number of distinct magmatic units, each a few hundred meters thick [e.g., *Suhr et al.*, 2008; *Natland and Dick*, 2002]; their lateral extent is not constrained. Differences in chemistry between units could affect velocities with a possible range of expected effect due to, for example, Mg# variability of up to 0.5 km/s [e.g., *Jacobs et al.*, 2007]. Another factor contributing to the shallow velocity structure is porosity, in this setting most likely associated with fracturing of the rock during unroofing/faulting. At ranges of 0.2–1.2 km along NOBEL9, velocities in the 100–300 mbsf depth interval are lower than those to the north. This area could be more intensely or pervasively fractured at seismic length scales than the area to the north. We note that the lower velocity ranges correspond to where a trough between corrugations on the dome occurs (Figure 8c).

[23] While our results suggest that seafloor scattering complicates reflection imaging in the local area around IODP Site 1309, we do not imply that the "D" reflector as mapped throughout the massif is a seafloor scattering phase. Both *Canales et al.* [2004] and *Singh et al.* [2004] show that there are significant reflectors in the northern central dome and on top of the southern ridge. The drilling results do not support the hypothesis that, in the immediate vicinity of the Site 1309 at least, the "D" reflector coincides with either a regional alteration front in a mainly peridotite footwall or that it marks a major subsurface detachment. It is possible that the "D" reflector is better described as the first in a series of deeper reflectors (see the supergather in Figure 4b of *Canales et al.* [2004]), rather than being an isolated single event that documents a major geologic break (whether actual fault zone or contrast in rock properties). The upper seismic reflector predicted by our reflectivity synthetic (Figure 4h) is associated with a drop in alteration intensity below the olivine-rich troctolite interval 280–360 mbsf. A similar coincidence of high alteration and olivine-rich troctolites occurs in the 1080~1200 mbsf interval and could give rise to deeper reflectors. Core sample velocities do not show a systematic relationship with primary lithology throughout Hole U1309D. We did find a local relation where core sample velocity, when determined at in situ pressure, suggests that olivine-rich troctolite in the interval 300–400 mbsf has velocities 0.5–1 km/s lower than nearby gabbroic samples. Log data correlates to some extent with overall alteration, showing an increase in velocity from the olivine-rich troctolite interval ~280–360 mbsf and an increase in wall rock resistivity at the base of both this and the deeper olivine-rich troctolite interval ~1080–1200 mbsf (Figure 4).

The strongest resistivity jump occurs just below a fault zone at 750 mbsf, coinciding with start of a rapid drop in overall alteration in the recovered core. Resistivity is sensitive to the bound water characteristic of alteration minerals, so that interface may well have an impedance contrast. However, neither our core samples nor the limited logging at greater depths provides convincing evidence of Vp, Vs, or density contrasts at this depth. Fluids within the fault zone at 750 mbsf might contribute, although seawater fraction would have to be sufficient to generate a reflection in 5–30 Hz MCS across a zone of thickness 10–20 m at this depth.

[24] In summary, seismic data in the vicinity of IODP Site 1309, including seafloor refraction, local MCS recordings, and borehole logging, can be modeled with a single, self-consistent velocity structure. Refraction data constrain a thin, shallowmost layer with velocity $\leq$3 km/s. All data indicate that velocities in the $\sim$200–500 mbsf interval averages 5.6 km/s and $\sim$6 km/s in the $\sim$500–800 mbsf interval. These velocities correspond to gabbroic lithologies that are moderately fractured and altered, consistent with the material recovered from Hole U1309D. Lateral variation in velocity of up to 1 km/s is documented over distances on the order of several hundred meters. The scale of this variation is comparable to downhole velocity changes that tend to correlate with changes in extents of alteration. Impedance contrasts correspond, in at least some cases, with rapid downhole variations in overall alteration but other factors, that warrant additional study (subsurface fault zones?), may also contribute to the apparent reflectivity imaged by the MCS.

Acknowledgments

[25] This research used samples and data provided by the Integrated Ocean Drilling Program (IODP). Support for this study was provided by JOI to JAC, DKB, and AH (grants T304B22, T305A22, and T305A1 respectively). John Diebold provided source signatures appropriate for modeling the MCS and VSP data. Discussions with Alistair Harding provided additional perspective and suggestion for a couple of specific tests.

References

Blackman, D. K., et al. (2002), Geology of the Atlantis Massif (MAR 30°N): Implications for the evolution of an ultramafic oceanic core complex, *Mar. Geophys. Res.*, *23*, 443–469, doi:10.1023/B:MARI.0000018232.14085.75.

Blackman, D. K., B. Ildefonse, B. E. John, Y. Ohara, D. J. Miller, C. J. MacLeod, and Expedition Scientists (2006), Oceanic core complex formation, Atlantis Massif, in *Proceedings of the Integrated Ocean Drilling Program*, vol. 304/305, Ocean Drill. Program, College Station, Tex.

Blackman, D. K., R. C. Searle, and G. Karner (2008), Three-dimensional structure of oceanic core complexes: Effects on gravity signature and ridge flank morphology, Mid-Atlantic Ridge 30°N, *Geochem. Geophys. Geosyst.*, *9*, Q06007, doi:10.1029/2008GC001951.

Canales, J. P., B. E. Tucholke, and J. A. Collins (2004), Seismic reflection imaging of an oceanic detachment fault: Atlantis megamullion (Mid-Atlantic Ridge, 30°10′N), *Earth Planet. Sci. Lett.*, *222*, 543–560, doi:10.1016/j.epsl.2004.02.023.

Canales, J. P., B. E. Tucholke, M. Xu, J. A. Collins, and D. L. Dubois (2008), Seismic evidence for large-scale compositional heterogeneity of oceanic core complexes, *Geochem. Geophys. Geosyst.*, *9*, Q08002, doi:10.1029/2008GC002009.

Cann, J. R., D. K. Blackman, D. K. Smith, E. McAllister, B. Janssen, S. Mello, E. Avgerinos, A. R. Pascoe, and J. Escartin (1997), Corrugated slip surfaces formed at ridge-transform intersections on the Mid-Atlantic Ridge, *Nature*, *385*, 329–332, doi:10.1038/385329a0.

Carlson, R. L. (2004), Seismic properties of layer 2A at 11 Ma: Results of a vertical seismic profile at Ocean Drilling Program Site 1243, *Geophys. Res. Lett.*, *31*, L17601, doi:10.1029/2004GL020598.

Carlson, R. L., and A. F. Gangi (1985), Effect of cracks on the pressure dependence of *P* wave velocities in crystalline rocks, *J. Geophys. Res.*, *90*, 8675–8684, doi:10.1029/JB090iB10p08675.

Carlson, R. L., and D. J. Miller (2004), Influence of pressure and mineralogy on seismic velocities in oceanic gabbros: Implications for the composition and state of the lower oceanic crust, *J. Geophys. Res.*, *109*, B09205, doi:10.1029/2003JB002699.

Carlson, R. L., D. K. Blackman, A. C. Harris, and J. A. Collins (2008), The effect of pressure on the in situ varation of velocity with depth in IODP Hole U1309D, *Eos Trans. AGU*, *89*(36), 331, doi:10.1029/2008EO360003.

Christeson, G., G. Purdy, and G. Fryer (1994), Seismic constraints on shallow crustal emplacement processes at the fast spreading East Pacific Rise, *J. Geophys. Res.*, *99*, 17,957–17,973, doi:10.1029/94JB01252.

Collins, J., J. Canales, and B. E. Tucholke (2003), Seismic velocity structure of mid-Atlantic ridge core complexes, *Geophys. Res. Abstr.*, *5*, 10390.

Dick, H. J. B., et al. (2000), A long in situ section of lower ocean crust: Results of ODP Leg 176 drilling at the southwest Indian Ridge, *Earth Planet. Sci. Lett.*, *179*, 31–51, doi:10.1016/S0012-821X(00)00102-3.

Escartín, J., C. Mével, C. J. MacLeod, and A. M. McCaig (2003), Constraints on deformation conditions and the origin of oceanic detachments, the Mid-Atlantic Ridge core complex at 15°45′N, *Geochem. Geophys. Geosyst.*, *4*(8), 1067, doi:10.1029/2002GC000472.

Harding, A. J., G. M. Kent, D. K. Blackman, S. Singh, and J.-P. Canales (2007), A new method for MCS refraction data analysis of the uppermost section at a Mid-Atlantic Ridge core complex, *Eos Trans. AGU*, *88*(52), Fall Meet. Suppl., Abstract S12A–03.

Ildefonse, B., D. K. Blackman, B. E. John, Y. Ohara, D. J. Miller, C. J. MacLeod, and I. E. S. Party (2007), Oceanic core complexes and crustal accretion at slow-spreading ridges, *Geology*, *35*, 623–626, doi:10.1130/G23531A.1.

Jacobs, A. M., A. J. Harding, and G. M. Kent (2007), Axial crustal structure of the Lau back-arc basin from velocity

modeling of multichannel seismic data, *Earth Planet. Sci. Lett.*, *259*, 239–255, doi:10.1016/j.epsl.2007.04.021.

Kelemen, P. B., E. Kikawa, D. J. Miller, and S. S. Party (2004), *Proceedings of the Ocean Drilling Program, Initial Report*, vol. 209, Ocean Drill. Program, College Station, Tex.

Kennett, B. L. N. (1983), *Seismic Wave Propagation in Stratified Media*, Cambridge Univ. Press, London.

Korenaga, J., W. Holbrook, G. Kent, P. Kelemen, R. Detrick, H.-C. Larsen, J. Hopper, and T. Dahl-Jensen (2000), Crustal structure of the southeast Greenland margin from joint refraction and reflection seismic tomography, *J. Geophys. Res.*, *105*, 21,591–21,614, doi:10.1029/2000JB900188.

MacLeod, C. J., et al. (2002), Direct geological evidence for oceanic detachment faulting: The Mid-Atlantic Ridge, *Geology*, *30*, 879–882, doi:10.1130/0091-7613(2002)030<0879:DGEFOD>2.0.CO;2.

Michibayashi, K., Y. Hariagane, J. Escartin, H. Delius, M. Linek, T. Hirose, T. Nozaka, and Y. Ohara (2008), Impermeable fault zone arising from high-T brittle shear within in situ oceanic crust, 30°N Mid-Atlantic Ridge, *Earth Planet. Sci. Lett.*, *275*, 348–354, doi:10.1016/j.epsl.2008.08.033.

Natland, J., and H. J. B. Dick (2002), *Proceedings of the Ocean Drilling Program, Scientific Results*, vol. 176, Ocean Drill. Program, College Station, Tex.

Nooner, S. L., G. S. Sasagawa, D. K. Blackman, and M. A. Zumberge (2003), Constraints on crustal structure at the Mid-Atlantic Ridge from seafloor gravity measurements made at the Atlantis Massif, *Geophys. Res. Lett.*, *30*(8), 1446, doi:10.1029/2003GL017126.

Okino, K., K. Matsuda, D. M. Christie, Y. Nogi, and K. Koizumi (2004), Development of oceanic detachment and asymmetric spreading at the Australian-Antarctic Discordance, *Geochem. Geophys. Geosyst.*, *5*, Q12012, doi:10.1029/2004GC000793.

Singh, S. C., J. A. Collins, J. P. Canales, B. E. Tucholke, and R. S. Detrick (2004), New insights into serpentinization at Atlantis Massif, *Eos Trans. AGU*, *85*(47), Fall Meet. Suppl., Abstract V23B–0628.

Smith, D. K., J. R. Cann, and J. Escartin (2006), Widespread active detachment faulting and core complex formation near 13 degrees N on the Mid-Atlantic Ridge, *Nature*, *442*, 440–443, doi:10.1038/nature04950.

Suhr, G., E. Hellebrand, K. Johnson, and D. Brunelli (2008), Stacked gabbro units and intervening mantle: A detailed look at a section of IODP Leg 305, Hole 1309D, *Geochem. Geophys. Geosyst.*, *9*, Q10007, doi:10.1029/2008GC002012.

Tucholke, B. E., and J. Lin (1994), A geological model for the structure of ridge segments in slow spreading ocean crust, *J. Geophys. Res.*, *99*, 11,937–11,958, doi:10.1029/94JB00338.

Tucholke, B. E., J. Lin, and M. C. Kleinrock (1998), Megamullions and mullion structure defining oceanic metamorphic core complexes on the Mid-Atlantic ridge, *J. Geophys. Res.*, *103*, 9857–9866, doi:10.1029/98JB00167.

Willson, S., A. C. Harris, R. L. Carlson, and D. K. Blackman (2007), Compressional-wave velocities of discrete samples at in-situ pressures from IODP Hole U1309D, *Eos Trans. AGU*, *88*(47), Fall Meet. Suppl., Abstract T53B–1303.

Zelt, C. A., and R. B. Smith (1992), Seismic travel-time inversion for 2-D crustal velocity structure, *Geophys. J. Int.*, *108*, 16–34, doi:10.1111/j.1365-246X.1992.tb00836.x.